A robust relativistic quantum two-level system with edge dependent currents and spin polarization

Xu, Hongya; Huang, Liang; Lai, Ying-Cheng

Published in:
Europhysics Letters

Publication date:
2016

Document Version
Peer reviewed version

A robust relativistic quantum two-level system with edge-dependent currents and spin polarization

HONGYA XU[1] , LIANG HUANG[2] , YING-CHENG LAI[1,3]

[1] *School of Electrical, Computer and Energy Engineering, Arizona State University, Tempe, Arizona 85287, USA*
[2] *Institute of Computational Physics and Complex Systems, and Key Laboratory for Magnetism and Magnetic Materials of MOE, Lanzhou University, Lanzhou, Gansu 730000, China*
[3] *Department of Physics, Arizona State University, Tempe, Arizona 85287, USA*

PACS `05.45.Mt` – Quantum chaos
PACS `73.23.Ra` – Persistent current
PACS `03.65.Pm` – Relativistic wave equations

Abstract – We consider a class of relativistic quantum systems of ring geometry with mass confinement, subject to a magnetic flux. Such a system supports a family of boundary modes with edge-dependent currents and spin polarization as the spinor-wave analog of the whispering galley modes. While these states are remarkably robust against random scattering, boundary deformations and/or bulk disorders can couple the two oppositely circulating base states. Superposition of the two states can be realized by sweeping an external magnetic flux. We also address the issue of decoherence and articulate a possible experimental scheme based on 3D topological insulators.

Introduction. Two-level systems are fundamental not only to the development of quantum mechanics [1], but also to quantum information processing and computing [2]. Exploiting various physical systems to realize two-level operation has been an active area of research for a few decades [3–5]. Among various types of two-level systems, superconducting and semiconductor-based systems are of particular interest [6]. A basic requirement for an effective two-level system is that it provides two controllable states such as the direction of the circulating currents on a ring, the charge states in a double quantum dot, and the electron spin. The performance of the device is affected by the coupling of these states with the environment and by their robustness against material defects or various types of random interactions. For example, two-level operation in a double quantum dot system is sensitive to charge noise and electrostatic fluctuations induced by interface roughness or bulk defects [7]. It is of general and continuous interest to articulate and develop two-level systems that are robust against random scattering and weak direct environmental coupling.

Recent years have witnessed a rapid growth of interest in Dirac materials [8] such as graphene [9–15], topological insulators (TIs) [16], molybdenum disulfide (MoS_2) [17,18], HITP [$Ni_3(HITP)_2$] [19], and topological Dirac semimetals [20,21]. A common feature of these materials is that the electronic motions can be approximately described by the Dirac equation, with physical properties that are not usually seen in conventional semiconductor materials. Appealing features of these materials include the emergence of topologically protected quantum states and long-range phase coherence [22], making them potential candidate for solid state two-level systems. Theoretical schemes have been proposed for graphene [23, 24], topological insulators [25], and more recently the monolayer transitional metal dichalcogenides [26].

In this paper, we present a two-level system based on a class of relativistic quantum modes, the Dirac spinor-wave analog of the whispering galley modes (WGMs). In particular, we consider the setting where a massless Dirac fermion is confined within a finite domain of ring topology, subject to a perpendicular magnetic flux at the center [23]. The confinement can be generated from a mass potential, which can be experimentally realized using ferromagnetic insulators [27]. A remarkable feature of the WGM type of spinor waves in the ring geometry is that they appear in pairs: one along the inner and another along the outer boundaries with oppositely circulating currents and spin polarizations, effectively forming a two-level relativistic quantum system. This Dirac system has peculiar spin textures as the coupling between the spin and current (momentum) constrains the spin directions into the plane transverse to the interface. The inner and outer states can be changed through tuning of the strength of the external magnetic field. The relativistic quantum two-level system is extremely robust against random scattering caused by boundary roughness and/or bulk electric disorders. Due to the breaking of the time-reversal symmetry (TRS) by the mass term, an insulator region is created. Based on the metal-insulator step junctions formed by spatially dependent mass potential in 2D Dirac fermion systems, we present an analytic argument to understand the origin of the robustness and the edge-dependent current/spin polarizations. A counter-intuitive feature is that, the inevitable boundary roughness and/or bulk defects are in fact desired, as they serve to introduce a finite coupling between the states, which is necessary for generating coherent oscillations through non-adiabatic sweeping of the external magnetic flux. We address the issue of decoherence and propose an experimental realization using 3D topological insulators (TIs). Our decoherence analysis based on a spin-boson model indicates that, for example, for a ring size of 100 nm, the quantum quality factor can be on the order of 10^4. Moreover, due to the TRS breaking confinement, our two-level system is less sensitive to electrostatic fluctuations than those based on conventional split-gate electrodes.

In the following, we first formulate a theoretical model and propose our relativistic quantum two-level system based on Dirac WGMs. We next demonstrate robustness and coherence of the system against random scatterings, and provide a physical explanation. We then address the issue of decoherence and finally conclude the work by articulating a feasible scheme for experimental realization.

Dirac Hamiltonian and two-level operation. We consider a 2D Dirac ring threaded by a magnetic flux Φ, as shown in Fig. 1(a). The Hamiltonian is

$$\hat{H}_D = \hbar v \hat{\boldsymbol{\sigma}} \cdot (-i\boldsymbol{\nabla} + e\boldsymbol{A}) + M(\boldsymbol{r})\hat{\sigma}_z, \tag{1}$$

where v is the Fermi velocity, $\hat{\boldsymbol{\sigma}} = (\hat{\sigma}_x, \hat{\sigma}_y)$ and $\hat{\sigma}_z$ are the Pauli matrices. The vector potential is $\boldsymbol{A}(\boldsymbol{r}) = (\Phi/2\pi r)\hat{\boldsymbol{e}}_\theta$ in the polar coordinates, with the magnetic field given by $\boldsymbol{B} = \alpha\Phi_0\delta(\boldsymbol{r})\hat{\boldsymbol{e}}_z$. The dimensionless quantum flux parameter is $\alpha = \Phi/\Phi_0$ with $\Phi_0 = 2\pi/e$ being the flux quantum. The mass confinement term $M(\boldsymbol{r})$ is zero inside the ring domain and infinity elsewhere, giving rise to the hard-wall boundary conditions [28,29]:

$$[1 - \mathrm{sgn}(M)\hat{\boldsymbol{n}}_\perp \cdot \hat{\boldsymbol{\sigma}}]\psi = 0, \tag{2}$$

where $\hat{\boldsymbol{n}}_\perp$ denotes the unit tangent vector at the boundaries and $\psi = [\psi_1, \psi_2]^{\mathrm{T}}$ is the eigenspinor.

In the polar coordinates, the kinetic part of the Hamiltonian Eq. (1) reads

$$v\hat{\boldsymbol{\sigma}} \cdot (-i\boldsymbol{\nabla} + e\boldsymbol{A}) = -iv\left[\hat{\sigma}_r\partial_r + \hat{\sigma}_\theta\frac{1}{r}(\partial_\theta + i\alpha)\right], \tag{3}$$

where $\hat{\sigma}_r = \hat{\sigma}_x\cos\theta + \hat{\sigma}_y\sin\theta$ and $\hat{\sigma}_\theta = -\hat{\sigma}_x\sin\theta + \hat{\sigma}_y\cos\theta$. For a circularly symmetric ring, $\hat{H}_D$ commutes with the the total angular momentum ($\hat{J}_z = -i\partial_\theta + \hat{\sigma}_z/2$). The corresponding eigenspinors ψ thus have the following form

$$\psi_l(\boldsymbol{r}) = \exp[i(l - 1/2)\theta]\begin{pmatrix} \varphi_l(r) \\ i\varphi_{l+1}(r)\exp(i\theta) \end{pmatrix}, \tag{4}$$

with

$$\varphi_l(r) = \mathcal{N}\left(H^{(1)}_{\bar{l}-1/2}(\kappa r) + \beta H^{(2)}_{\bar{l}-1/2}(\kappa r)\right), \tag{5}$$

where $\mathcal{N}$ denotes the normalization constants, $\bar{l} = l + \alpha$ ($l = \pm 1/2, \pm 3/2, \cdots$ are the eigenvalues of $\hat{J}_z$), $H^{(1,2)}_\nu$ are Hankel functions of the (first, second) kind and $\kappa = |E|R/v$. The eigenstates and eigenvalues are determined by imposing the boundary condition Eq. (2).

Using the local charge current density $\boldsymbol{j} = v\psi^\dagger\hat{\boldsymbol{\sigma}}\psi$, we can obtain an expression for the edge current $\boldsymbol{j}(\boldsymbol{r}_B) = 2v|\psi_1|^2\mathrm{sgn}(M)\hat{\boldsymbol{n}}_\perp$ and show that it is polarized along the edges, *clockwise* for the inner and *counterclockwise* for the outer boundaries. Adopting the spin operator in the Hamiltonian as [25] $\hat{\boldsymbol{S}} = 1/2(\hat{\sigma}_y, -\hat{\sigma}_x, \hat{\sigma}_z)$ we obtain that the edge spin direction $\boldsymbol{S}(\boldsymbol{r}_B) = |\psi_1|^2\mathrm{sgn}(M)\hat{\boldsymbol{n}}_\parallel$ is parallel to the outer normal vector $\hat{\boldsymbol{n}}_\parallel$, where $\boldsymbol{r}_B$ specifies the coordinates of the boundary points. The detailed form of the confinement potential $M(\boldsymbol{r})$ and disorders in the system will affect the magnitude of the edge charge current/spin but not the polarization properties. This current/spin polarization characteristic makes the system a potential candidate for relativistic quantum two-level operation.

For two-level operation, in addition to the well defined current/spin polarization characteristic, it is necessary to lift the state degeneracy in the circular symmetric ring [23]. Intuitively, this can be accomplished through the boundary roughness of the ring or defects in the bulk, with the current/spin polarization characteristic well maintained. Without loss of generality, we consider a class of deformed Dirac rings with shape being a conformal image of the circular-symmetric ring so that the eigenstates can be determined efficiently and accurately [30,31]. The conformal mapping of the circular ring domain z is given by $w(z) = \sum_n c_n z^n$ where $n = 5$ and the coefficient vector is given by $\boldsymbol{c} = [1, 0.05g, 0, 0, 0.18g\exp(i\delta)]$, $\delta \in [0, 2\pi)$, and $g \in [0, 1]$ is the deformation parameter that opens the gap at anti-level crossing. For relatively large deformation, e.g., $g \gtrsim 0.5$, bottlenecks along the boundary occur, leading to chaotic behavior in the classical ray dynamics and random scattering in the quantum regime. Conventional wisdom stipulates that the current/spin polarizations along the inner and outer boundaries would be suppressed or even eliminated. Remarkably, we find that the (deformed) Dirac ring system and the associated polarized properties in the charge current and spin texture can persist in an extremely robust manner, as shown in Fig. 1, where panel (b) shows the lowest few energy levels versus α, panels (c) and (d) show, for the two energy values indicated in b, the associated spinor eigenstates. The states are radially localized at the ring edges with opposite propagating edge currents, forming the spinor-wave-analog of the WGMs. The coupling between the spin and current (momentum) constrains the spatial spin texture into the $S_r - S_z$ plane with $S_r = \sigma_y \cos\theta - \sigma_x \sin\theta$. From Figs. 1(c) and 1(d), we see that, at the boundaries, the spinors are planar with opposite polarization for the inner and outer states. Further, the oppositely circulating currents lead to opposite magnetic response in that the inner and outer WGM-like states are *diamagnetic* and *paramagnetic*, respectively. In absence of coupling between these WGM states (e.g., in absence of any random boundary scattering or bulk disorder), a level-crossing structure will arise as the magnetic flux is varied.

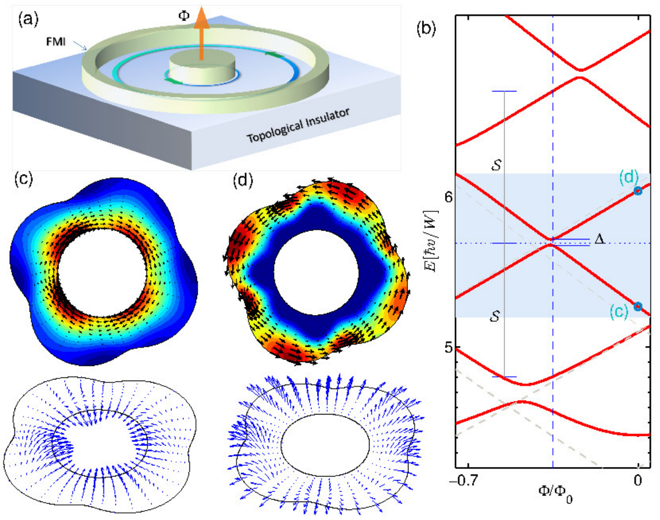

Fig. 1: (a) Proposed relativistic quantum two-level system patterned as a ring domain through the deposition of a ferromagnetic insulator (e.g., EuS) on the surface of the 3D TI, where a controllable mass potential is created through local exchange coupling (the proximity effect). (b) For $g = 0.5$, energy levels versus α, where the dashed lines show the circularly symmetric case for comparison. (c,d) The corresponding electronic densities and the associated charge current distribution (upper panels) and spin texture (lower panels) of the two adjacent Dirac WGMs indicated by the open circles in (b).

A pair of WGM-like states traveling along the inner and outer boundaries define effectively a two-level system. For simplicity, we use the symbols $|\circlearrowleft\rangle$ and $|\circlearrowright\rangle$ to denote the two states, with the respective energy levels $E_{\curvearrowleft}(\alpha)$ and $E_{\curvearrowright}(\alpha)$. About the level anti-crossing point [i.e., minimal-gap position in Fig. 1(b)], the states $|\circlearrowleft\rangle$ and $|\circlearrowright\rangle$ are coupled and superposed with approximately equal amplitude. An example of the "on-off" curves is shown in Fig. 2(a). Rabi oscillations can be generated by varying the magnetic flux in a nonadiabatic manner. Specifically, the single flux-tunable two-level system can be described by the following 2×2 effective Hamiltonian in the pseudo-spin representation as

$$\hat{H}_{\text{two level}} = -(\tilde{\varepsilon}/2)\hat{\tau}_z - (\Delta/2)\hat{\tau}_x, \tag{6}$$

where $\hat{\tau}_{x,z}$ are Pauli matrices in the pseudo-spin base of $|\circlearrowleft\rangle$ and $|\circlearrowright\rangle$, and $\varepsilon = |E_{\curvearrowleft}(\alpha) - E_{\curvearrowright}(\alpha)|$. The level detuning $\tilde{\varepsilon} = \varepsilon - \varepsilon_0$ can be adjusted by changing α, where ε_0 characterizes the displacement with respect to the uncoupled situation. The tunnel coupling parameter Δ is the anti-crossing energy, which can be tuned by varying the boundary deformation parameter g or the bulk disorder strength. Non-adiabatic transitions between $|\circlearrowleft\rangle$ and $|\circlearrowright\rangle$ can be realized through non-adiabatic tuning of α such that the level detuning changes from $|\tilde{\varepsilon}| \gg \Delta$ to $\tilde{\varepsilon} = 0$ (i.e. $\varepsilon = \varepsilon_0$), driving the system from a pure $|\circlearrowleft\rangle$ (or $|\circlearrowright\rangle$) state to the minigap position. This induces Rabi oscillations between $|\circlearrowleft\rangle$ and $|\circlearrowright\rangle$ at the angular frequency of $\Delta/2$: $\cos(\Delta t/2)|\circlearrowleft\rangle - i\sin(\Delta t/2)|\circlearrowright\rangle$.

We note that the effect of additional mass term (dynamical gap) generation induced by such a dynamical flux is irrelevant in practice, as that requires an *off-resonant* circularly polarized irradiation (laser) or a high-frequency analog driving signal input [e.g., about 100 meV ($\sim 10^{15}$ Hz) - see the work [32], and references therein]. In our system, the time-dependent gauge potential induced by the applied dynamic magnetic flux has a different form from that generated by the circularly polarized laser field, and the relevant operation (driving) frequency is on the same order of magnitude of the energy spacing between the two adjacent WGM states. The energy requirement is 1 meV for a real ring size (say 100 nm). As a result, the additional mass term can be neglected. The $\delta(r)$ field adopted in our analysis is for theoretical simplicity only. Insofar as the applied magnetic flux is confined within the inner ring boundary, there is no essential difference in the final results. In experimental implementation, it may be feasible to generate a magnetic flux of finite size confined within the inner ring boundary.

We now provide additional reasoning that our Dirac ring system can effectively be approximated as a two-level system. When two specific levels are chosen, the level spacings from them to the lower or higher states should be much larger than the two-level splitting energy to prevent information leaking [33]. Our system fulfills this requirement. In particular, consider the two-level profile consisting of a pair of WGM-like states as indicated in Fig. 1(b) (open circles). We obtain that the level splitting is about $\Delta \sim 0.04\hbar v/W$, but the smallest level spacing from other states is $\mathcal{S} \sim \hbar v/W$, which is about 25 times larger than the former. For a realistic sample size, e.g., $W = 100$ nm, we get $\mathcal{S} \sim 5$meV $\simeq 60$K and $\Delta \sim 0.2$meV $\simeq 2.5$K $\ll \mathcal{S}$. This means that the chosen two-level profile is effectively decoupled from other levels of the system. The splitting energy Δ in fact defines an effective temperature T under which the dephasing effect of thermal noise can be ruled out. In this sense, through tuning of the Fermi energy near a desired position as indicated by the dotted blue horizontal line in Fig. 1(b), for low temperatures (e.g., $k_B T \ll \Delta$) we obtain a robust two-level quantum system for some proper value of the magnetic flux. Note that our theoretical proposal is based on the low energy model of 3D TIs, so it is adequate to focus on the low-lying states

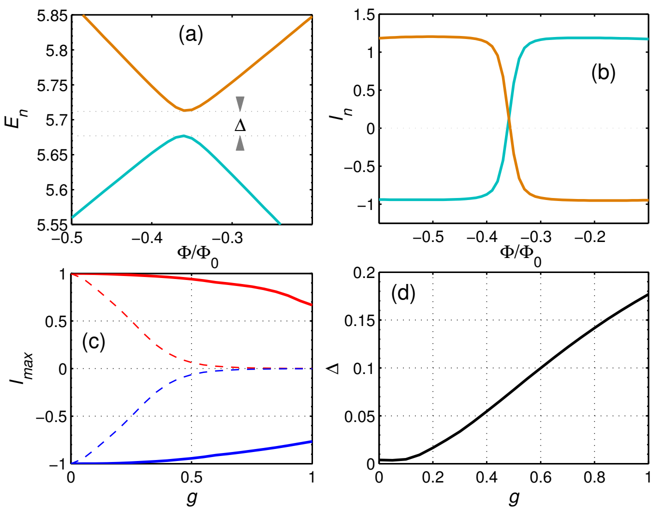

Fig. 2: Illustration of a flux-tunable two-level system based on a pair of Dirac WGMs: (a,b) “on-off” curves, and (c,d) the circulating current amplitudes and the anti-crossing energy as a function of the deformation parameter g, respectively. The dashed lines in (c) are for the non-relativistic counterpart of our system.

only.

Robustness against random scattering. The quantum states in our system, which are the Dirac spinor-wave analog of WGMs with opposite circulating currents and spin polarizations, are far superior to the same setup in nonrelativistic, semiconducting rings. This can be argued, as follows. Say we calculate the slope of the states $I_n = -\partial E_n/\partial\alpha$ (the persistent current [34–52]), which measures the degree of coherence in terms of the states' ability to maintain circulation. The slope will have large and near zero values for circulating and angularly localized states, respectively. From Fig. 2(b), we see that the Dirac WGMs have quite large circulating currents. Remarkably, as the deformation strength g is increased, the corresponding current amplitudes denoted by the solid thick lines in Fig. 2(c) decrease much more slowly. For comparison, we calculate the corresponding behaviors for the non-relativistic counterpart of our system [the thin dashed lines in Fig. 2(c)], where the current amplitude decays much faster. Figure 2(d) shows that the mingap Δ increases with the deformation strength g, which is reasonable as gap opening is typically more pronounced as some symmetry-breaking parameter is increased.

Taking advantage of the concept of persistent currents, we can analyze the characteristics of our Dirac ring system more explicitly using, e.g., the specific two-level profile as shown in Fig. 2(a). We define the parameter

$$\tilde{\varepsilon} \sim 2I_m(\alpha - \alpha_c), \tag{7}$$

where α_c is the position of the anti-crossing and I_m denotes the maximum absolute amplitude of the persistent current carried by the quantum states. For successful two-level implementation, I_m should be robust against various kinds of random perturbations. To be concrete, we consider a generic type of perturbation, namely, irregular boundary deformations and demonstrate that the quantum states are stable because they are robust *relativistic* WGM-like states (the nonrelativistic counterparts are generally not robust against random scattering). Physically, the boundary deformations can be conformally mapped into a circular-symmetric ring domain as impurities. Our two-level system should thus be robust against random perturbations induced by, e.g., TRS breaking disorders. Remarkably, the boundary deformations introduce the necessary coupling between the states, which can be characterized by Δ as a function of deformation parameter g. From Figs. 2(a)-(d), we can estimate that, for the case of most severe deformation, i.e., $g = 1$, the maximum level detuning $\tilde{\varepsilon}_M \sim 0.88\hbar v/W$ is still about five times larger than the energy splitting $\Delta \sim 0.18\hbar v/W$, suggesting the effectiveness of the two-level approximation.

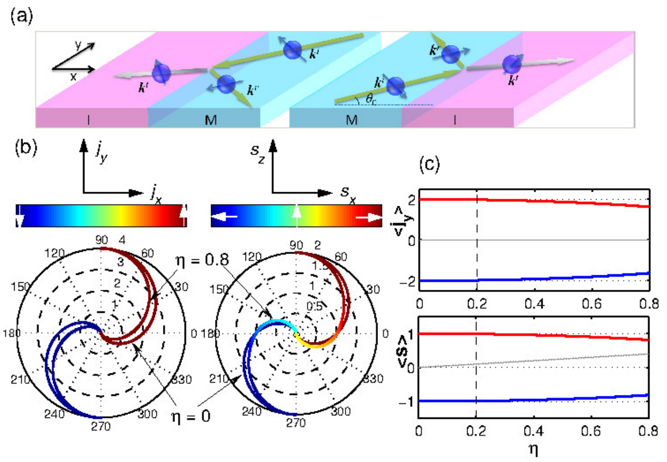

Fig. 3: Physical mechanism of robust Dirac WGMs: (a) a 2D step junction with IM (left) and MI (right) configurations, where the junction interface is located at $x = 0$, (b) interface current orientation (j_x, j_y) (left panel) and spin texture (S_x, S_z) (right panel) versus the incident angle θ_0 and the relative energy η, where $\theta_0 \in [-\pi/2, \pi/2]$ and $\theta_0 \in [\pi/2, 3\pi/2]$ for MI and IM, respectively. The results for different values of η are indicated. (c) Averaged transverse electric current (top panel) and spin (bottom panel) versus the incident relative energy η.

To understand the physical mechanism of robust Dirac WGMs, we analyze the relativistic quantum behaviors of a particle in a 2D step junction system with metal-insulator (MI) and insulator-metal (IM) configurations formed by a spatial-dependent mass potential, as shown in Fig. 3(a). The insulator region can be created experimentally with a finite constant mass potential $M = M_0$ (since we only consider the lowest few levels), while the metal region with zero band gap hosts massless Dirac fermions. An incoming plane wave $|k^i\rangle$ from the metal to the insulator regions with the incident angle θ and energy $E = v|k|$ inside the mass gap $|M_0| > E$ is reflected to state $|k^r\rangle$, together with an evanescent state $|k^t\rangle$ in the insulator region. Solving the Dirac equation together with the boundary conditions (Appendix), we obtain the associated local charge current density and spin orientation as

$$\begin{aligned} j_x &= 0, \\ j_y &= v\frac{4\tau\cos^2\gamma}{\tan\beta} \times \exp(-2qx), \end{aligned} \tag{8}$$

and

$$\begin{aligned} S_x &= \frac{2\tau\cos^2\gamma}{\tan\beta} \times \exp(-2qx), \\ S_y &= 0, \\ S_z &= \frac{\cos^2\gamma}{\sin^2\beta}\cos(2\beta) \times \exp(-2qx), \end{aligned} \tag{9}$$

where

$$\begin{aligned} \tan\beta &= |(vq + E\sin\theta_0)/(M_0 + E)|, \\ \tan\gamma &= (1 - \tau\tan\beta\sin\theta_0)/(\tau\tan\beta\cos\theta_0), \\ \tau &= \mathrm{sgn}(M_0 q), \\ vq &= \pm\sqrt{M_0^2 - (E\cos\theta_0)^2}, \end{aligned}$$

with the $\pm$ signs denoting the propagating directions of the incident wave from the metal region (corresponding to the MI and IM configurations, respectively). We see that spin is perpendicular to the current direction, which is responsible for the strong spin-orbit coupling associated with the surface states of 3D TIs. The transverse current j_y and the constrained spin orientation (S_x, S_z) are both functions of the relative incident energy ratio $\eta = E/M_0$ and the incident angle θ_0 with respect to the x-axis. An interesting feature is that the signs of j_y and S_x are simply determined by those of mass M_0 and q. Restricting our consideration to $M_0 > 0$, we see that both j_y and S_x are anti-symmetric with respect to the transformation of $q \to -q, \theta_0 \to \theta_0 + \pi$. As a result, j_y and S_x are positive/negative for the MI/IM junction, leading to persistent positive/negative transverse current and left/right spin polarization at the junction interfaces when all possible incident angles are taken into account. This is the situation where there are transverse Hall currents *without* external magnetic fields, and the directions of the currents can be controlled by changing the configuration of the junction. More physical insights into these peculiar currents can be gained by considering the case of hard wall confinement: $\eta \ll 1$. At the interface, we have

$$\begin{aligned} j_y &\to 2v(\tau + \sin\theta_0), \\ S_x &\to (\tau + \sin\theta_0), \\ S_z &\to 0. \end{aligned}$$

That is, the spin becomes fully in-plane polarized ($\leftarrow$ or $\rightarrow$), as shown in Fig. 3(b). Averaging over all the incident angles $\theta_0 \in [-\pi/2, \pi/2]$ for MI ($[\pi/2, 3\pi/2]$ for IM), we obtain

$$\langle j_y\rangle = \frac{1}{\pi}\lim_{\eta\to 0}\int_{-\pi/2}^{\pi/2} d\theta_0 j_y(\eta,\theta_0) = 2v\tau, \tag{10}$$

and

$$\langle S_x\rangle = \frac{1}{\pi}\lim_{\eta\to 0}\int_{-\pi/2}^{\pi/2} d\theta_0 s_x(\eta,\theta_0) = \tau. \tag{11}$$

As shown in Fig. 3(c), both average values are half of their maximum values in magnitude but the currents and spins are opposite in direction for the MI and IM configurations.

Decoherence. For a quantum two-level system to be practically useful, the dephasing time τ_φ and the relaxation time τ_r need to be much larger than the Rabi period (operation time scale) $\tau_{op} = 4\pi/\Delta$. Our relativistic quantum states are spin polarized WGMs, so they are less sensitive to nonmagnetic perturbations, such as electrostatic fluctuations, than those based on conventional split-gate electrodes [53]. At low temperatures $k_B T \ll \Delta$, decoherence mainly comes from the measurement process. We use the standard spin-boson model (SBM) to calculate the decoherence time caused by the coupling to the measurement device (e.g., a superconducting quantum interference device - SQUID), which has been used to assess decoherence in flux based, nonrelativistic quantum systems of mesoscopic semiconducting [54] or superconducting rings [55]. For a system at the bath temperature T, the energy relaxation time is

$$\tau_r^{-1} = 0.5J\left(\frac{\mu}{\hbar}\right)\coth\left(\frac{\mu}{2k_B T}\right)\sin^2\Omega, \tag{12}$$

and the phase-decoherence time is

$$\tau_\varphi^{-1} = \frac{\tau_r^{-1}}{2} + 2\pi\xi k_B T\cos^2\Omega/\hbar, \tag{13}$$

where the level spacing is $\mu = \sqrt{\bar{\varepsilon}^2 + \Delta^2}$, $\Omega = \tan^{-1}(\Delta/\mu)$ is the mixing angle, $J(\omega)$ is a spectral density function characterizing the environment, and the dimensionless dissipation parameter is defined as

$$\xi = \lim_{\omega\to 0} J(\omega)/2\pi\omega. \tag{14}$$

For $\mu \gg k_B T$ and assuming that the environment can be treated as an Ohmic bath [i.e., $J(\omega) \propto \omega$], we have

$$\tau_r^{-1} \simeq \pi\xi\mu\sin^2\Omega/\hbar, \tag{15}$$

with the damping parameter given by

$$\xi \simeq (2\pi/\hbar)(\mathcal{M}I/\Phi_0)^2 I_{sq}^2\tan^2[f(L_J^2/R_l)k_B T], \tag{16}$$

where $\mathcal{M}$ is the mutual inductance coefficient between the two-level system and the measuring SQUID, I and I_{sq} are the respective circulating currents. The SQUID is effectively an inductor of inductance

$$L_J = (\hbar/2e)/\sqrt{4I_c^2\cos^2 f - I_{sq}^2} \tag{17}$$

and is driven by a magnetic flux f with the flux-tunable critical current I_c. The quantity R_l is used to model the real part of the impedance resulting from non-ideal wirings to the SQUID. Adopting the same parameters for the measuring device as in Ref. [56], we obtain $\tau_r \sim 45$ ns and $\tau_\varphi \sim 59$ ns at 300 mK for our Dirac ring of size ~ 100 nm. In realistic situations the Ohmic environment assumption cannot adequately describe all sources of decoherence, but these estimates provide a meaningful assessment of the system operation. In particular, level spacing in our system sets the operation time to be $\tau_{op} \sim 4$ ps, which is much less than τ_φ. The corresponding quantum quality factor can thus be quite large: on the order of 10^4, suggesting strongly that our two-level system can be tested experimentally and potentially useful for applications [57,58].

Conclusions. We conclude by presenting a potential experimental scheme to realize our robust relativistic two-level system. The key lies in the implementation of mass confinement, which can be accomplished using graphene or 3D TIs. For example, a controllable mass term can be created by depositing a ferromagnetic insulator (FMI) layer on the surface of a 3D TI [27]. Differing from graphene, the surface states of a 3D TI host Dirac fermions originated from a single Dirac cone, which is the case treated in this work. One possible scheme based on 3D TIs (Bi_2Se_3, $Pb_xSn_{1-x}Te$) is sketched in Fig. 1(a), where the material EuS (GdN or $Cr_2Ge_2Te_6$) can be used for the FMI cap layer and patterned to generate a ring geometry. System readout can be realized by measuring the sign of the flux generated by the circulating currents, using a separate SQUID magnetometer inductively coupled to the system. In practice, the current scanning SQUID technique allows one to filter the applied controlling flux from the one induced by the quantum states [59]. Two or more such system can also be coupled by means of the induced flux, making it possible to develop gates or even a network of Dirac two-level system. We emphasize the surprising feature of our two-level system: during various stages of the fabrication process boundary imperfections and/or bulk disorders are inevitable, but they are counterintuitively beneficial for our system because they provide the necessary coupling between the two oppositely circulating boundary states. A key merit of our proposal lies in its relativistic quantum nature, due to the strong current interest in Dirac materials and their unconventional electronic properties.

* * *

This work was supported by AFOSR under Grant No. FA9550-15-1-0151. LH was supported by NSFC under Grant No. 11422541.

Appendix: Derivation of Eq. (8) and Eq. (9). – Imposing the continuity of the waves at the junction interface $x = 0$ [Fig. 3(a)], i.e.

$$|k^i\rangle + R|k^r\rangle = T|k^t\rangle, \tag{18}$$

we obtain the undetermined coefficients

$$R = \exp\left[i(2\gamma + \theta_0 - \pi/2)\right], \tag{19}$$

and

$$T = \frac{2\cos\gamma}{\tau\sin\beta}\exp\left[i(\gamma + \theta_0/2)\right], \tag{20}$$

with the auxiliary parameters β and γ satisfying

$$\tan\beta = \left|\frac{vq + E\sin\theta_0}{M_0 + E}\right|,$$

and

$$\tan\gamma = \frac{1 - \tau\tan\beta\sin\theta_0}{\tau\tan\beta\cos\theta_0},$$

where $\tau = \mathrm{sgn}(M_0 q)$, $vq = \pm\sqrt{M_0^2 - (E\cos\theta_0)^2}$ with the sign $\pm$ denoting the propagating directions of the incident wave from the metal region and hence corresponding to the MI/IM configurations, respectively. The wavefunction in the insulator region can thus be expressed explicitly as

$$\psi^t = \langle r|k^t\rangle = \frac{T}{\sqrt{2}}\begin{pmatrix} -i\cos\beta \\ \tau\sin\beta \end{pmatrix}\exp(-qx) \times e^{i\frac{E\sin\theta_0}{v}y}. \tag{21}$$

The associated local charge current density and spin orientation are determined by the corresponding definitions $\boldsymbol{j} = v\psi^\dagger\hat{\boldsymbol{\sigma}}\psi$ and $\boldsymbol{S} = \psi^\dagger\hat{\boldsymbol{S}}\psi$, leading to Eqs. (8) and (9).

REFERENCES

[1] Feynman R. P., *The Feynman Lectures on Physics Volume III* (Addison-Wesley, Reading, Massachusetts) 1963.

[2] Nielsen M. A. and Chuang I. L., *Quantum Computation and Quantum Information* (Cambridge University Press, Cambridge, UK) 2000.

[3] Loss D. and DiVincenzo D. P., *Phys. Rev. A*, **57** (1998) 120.

[4] You J. Q. and Nori F., *Phys. Today*, **58** (2005) 42.

[5] Medford J., Beil J., Taylor J. M., Rashba E. I., Lu H., Gossard A. C. and Marcus C. M., *Phys. Rev. Lett.*, **111** (2013) 050501.

[6] Paladino E., Galperin Y. M., Falci G. and Altshuler B. L., *Rev. Mod. Phys.*, **86** (2014) 361.

[7] Casati G., Shepelyansky D., Zoller P. and Benenti G., *Quantum Computers, Algorithms and Chaos* (IOS Press, Bologna, Italy) 2006.

[8] Neto A. H. C. and Novoselov K., *Mater. Exp.*, **1** (2011) 10.

[9] Novoselov K. S., Geim A. K., Morozov S. V., Jiang D., Zhang Y., Dubonos S. V., Grigorieva I. V. and Firsov A. A., *Science*, **306** (2004) 666.

[10] Berger C., Song. Z. M., Li. T. B., Li X. B., Ogbazghi A. Y., Dai R. F. Z. T., Marchenkov. A. N., Conrad E. H., First P. N. and de Heer W. A., *J. Phys. Chem. B*, **108** (2004) 19912.

[11] Novoselov K. S., Geim A. K., Morozov S. V., Jiang D., Katsnelson M. I., Grigorieva I. V., Dubonos S. V. and Firsov A. A., *Nature*, **438** (2005) 197.

[12] Zhang Y. B., Tan Y. W., Stormer H. L. and Kim P., *Nature*, **438** (2005) 201.

[13] Neto A. H. C., Guinea G., Peres N. M. R. and andA. K. Geim K. S. N., *Rev. Mod. Phys.*, **81** (2009) 109.

[14] Peres N. M. R., *Rev. Mod. Phys.*, **82** (2010) 2673.

[15] Sarma S. D., Adam S., Hwang E. H. and Rossi E., *Rev. Mod. Phy.*, **83** (2011) 407.

[16] Hasan M. Z. and Kane C. L., *Rev. Mod. Phys.*, **82** (2010) 3045.

[17] Radisavljevic B., Radenovic A., Brivio J., Giacometti V. and Kis A., *Nat. Nanotech.*, **6** (2011) 147.

[18] Wang Q. H., Kalantar-Zadeh K., Kis A., Coleman J. N. and Strano M. S., *Nat. Nanotech.*, **7** (2012) 699.

[19] Sheberla D., Sun L., Blood-Forsythe M. A., S. Er C. R. W., Brozek C. K., Aspuru-Guzik A. and Dinca M., *J. Am. Chem. Soc.*, **136** (2014) 8859.

[20] Liu Z. K., Zhou B., Zhang Y., Wang Z. J., Weng H. M., Prabhakaran D., Mo S.-K., Shen Z. X., Fang Z., Dai X., Hussain Z. and Chen Y. L., *Science*, **343** (2014) 864.

[21] Liu Z. K., Jiang J., Zhou B., Wang Z. J., Zhang Y., Weng H. M., Prabhakaran D., Mo S.-K., Peng H., Dudin P., Kim T., Hoesch M., Fang Z., Dai X., Shen Z. X., Feng D. L., Hussain Z. and Chen Y. L., *Nature Materials*, **13** (2014) 677.

[22] Wehlingab T. O., Black-Schafferc A. M. and Balatskyd A. V., *Adv. Phys.*, **63** (2014) 1.

[23] Recher P., Trauzettel B., Rycerz A., Blanter Y. M., Beenakker C. W. J. and Morpurgo A. F., *Phys. Rev. B*, **76** (2007) 235404.

[24] Trauzettel B., Bulaev D. V., Loss D. and Burkard G., *Nat. Phys.*, **3** (2007) 192.

[25] Ferreira G. J. and Loss D., *Phys. Rev. Lett.*, **111** (2013) 106802.

[26] Kormányos A., Zólyomi V., Drummond N. D. and Burkard G., *Phys. Rev. X*, **4** (2014) 011034.

[27] Wei P., Katmis F., Assaf B. A., Steinberg H., Jarillo-Herrero P., Heiman D. and Moodera J. S., *Phys. Rev. Lett.*, **110** (2013) 186807.

[28] Berry M. V. and Mondragon R. J., *Proc. Roy. Soc. Lond. A*, **412** (1987) 53.

[29] McCann E. and Fal'ko V., *J. Phys. Condens. Matter*, **16** (2004) 2371.

[30] Xu H., Huang L., Lai Y.-C. and Grebogi C., *Phys. Rev. Lett.*, **110** (2013) 064102.

[31] Xu H., Huang L., Lai Y.-C. and Grebogi C., *Sci. Rep.*, **5** (2015) .

[32] Perez-Piskunow P. M., Usaj G., Balseiro C. A. and Torres L. E. F. F., *Phys. Rev. B*, **89** (2014) 121401.

[33] Mooij J. E. and Harmans C. J. P. M., *New J. Phys.*, **7** (2005) 219.

[34] Büttiker M., Imry Y. and Landauer R., *Physics Letters A*, **96** (1983) 365.

[35] Lévy L. P., Dolan G., Dunsmuir J. and Bouchiat H., *Phys. Rev. Lett.*, **64** (1990) 2074.

[36] Chandrasekhar V., Webb R. A., Brady M. J., Ketchen M. B., Gallagher W. J. and Kleinsasser A., *Phys. Rev. Lett.*, **67** (1991) 3578.

[37] Bleszynski-Jayich A. C., Shanks W. E., Peaudecerf B., Ginossar E., von Oppen F., Glazman L. and Harris J. G. E., *Science*, **326** (2009) 272.

[38] Bluhm H., Koshnick N. C., Bert J. A., Huber M. E. and Moler K. A., *Phys. Rev. Lett.*, **102** (2009) 136802.

[39] Castellanos-Beltran M. A., Ngo D. Q., Shanks W. E., Jayich A. B. and Harris J. G. E., *Phys. Rev. Lett.*, **110** (2013) 156801.

[40] Mailly D., Chapelier C. and Benoit A., *Phys. Rev. Lett.*, **70** (1993) 2020.

[41] Rabaud W., Saminadayar L., Mailly D., Hasselbach K., Benoît A. and Etienne B., *Phys. Rev. Lett.*, **86** (2001) 3124.

[42] Kleemans N. A. J. M., Bominaar-Silkens I. M. A., Fomin V. M., Gladilin V. N., Granados D., Taboada A. G., García J. M., Offermans P., Zeitler U., Christianen P. C. M., Maan J. C., Devreese J. T. and Koenraad P. M., *Phys. Rev. Lett.*, **99** (2007) 146808.

[43] Sivan U. and Imry Y., *Phys. Rev. Lett.*, **61** (1988) 1001.

[44] Cheung H.-F., Riedel E. K. and Gefen Y., *Phys. Rev. Lett.*, **62** (1989) 587.

[45] von Oppen F. and Riedel E. K., *Phys. Rev. Lett.*, **66** (1991) 84.

[46] Ambegaokar V. and Eckern U., *Phys. Rev. Lett.*, **65** (1990) 381.

[47] Schmid A., *Phys. Rev. Lett.*, **66** (1991) 80.

[48] Berkovits R. and Avishai Y., *Phys. Rev. Lett.*, **76** (1996) 291.

[49] Splettstoesser J., Governale M. and Zülicke U., *Phys. Rev. B*, **68** (2003) 165341.

[50] Sheng J. S. and Chang K., *Phys. Rev. B*, **74** (2006) 235315.

[51] Gudmundsson V., Tang C.-S. and Manolescu A., *Phys. Rev. B*, **67** (2003) 161301.

[52] Matos-Abiague A. and Berakdar J., *Phys. Rev. Lett.*, **94** (2005) 166801.

[53] Hayashi T., Fujisawa T., Cheong H. D., Jeong Y. H. and Hirayama Y., *Phys. Rev. Lett.*, **91** (2003) 226804.

[54] Zipper E., Kurpas M., Szelág M., Dajka J. and Szopa M., *Phys. Rev. B*, **74** (2006) 125426.

[55] Yu Y., Nakada D., Lee J. C., Singh B., Crankshaw D. S., Orlando T. P., Berggren K. K. and Oliver W. D., *Phys. Rev. Lett.*, **92** (2004) 117904.

[56] van der Wal C. H., andl C. J. P. M. Harmans F. K. W. and Mooij J. E., *Eur. Phys. J. B*, **31** (2003) 111.

[57] Makhlin Y., Schön G. and Shnirman A., *Rev. Mod. Phys.*, **73** (2001) 357.

[58] Bennett C. H. and DiVincenzo D. P., *Nature (London)*, **404** (2000) 247.

[59] Koshnick N. C., Bluhm H., Huber M. E. and Moler K. A., *Science*, **318** (2007) 1440.